

<sup>1</sup> **Variation of the solar magnetic flux spectrum during**  
<sup>2</sup> **solar cycle 23**

C. L. Jin and J. X. Wang

Key Laboratory of Solar Activity, National Astronomical Observatories, Chinese Academy of Sciences, Beijing 100012, China

arXiv:1312.5816v1 [astro-ph.SR] 20 Dec 2013

---

A20 Datun Road Chaoyang District, Beijing 100012, China(cljin@nao.cas.cn;  
wangjx@nao.cas.cn)

3 **Abstract.** By using the unique database of SOHO/MDI full disk mag-  
4 netograms from 1996 September to 2011 January, covering the entire solar  
5 cycle 23, we analyze the time-variability of the solar magnetic flux spectrum  
6 and study the properties of extended minimum of cycle 23. We totally iden-  
7 tify 11.5 million magnetic structures. It has been revealed that magnetic fea-  
8 tures with different magnetic fluxes exhibit different cycle behaviors. The mag-  
9 netic features with flux larger than  $4.0 \times 10^{19}$  Mx, which cover solar ac-  
10 tive regions and strong network features, show exactly the same variation  
11 as sunspots; However, the remaining 82% magnetic features which cover the  
12 majority of network elements show anti-phase variation with sunspots. We  
13 select a criterion that the monthly sunspot number is less than 20 to rep-  
14 resent the Sun's low activity status. Then we find the extended minimum  
15 of cycle 23 is characterized by the long duration of low activity status, but  
16 the magnitude of magnetic flux in this period is not lower than previous cy-  
17 cle. Both the duration of low activity status and the minimum activity level  
18 defined by minimum sunspot number show a century period approximately.  
19 The extended minimum of cycle 23 shows similarities with solar cycle 11, which  
20 preceded the mini-maxima in later solar cycles. This similarity is suggestive  
21 that the solar cycles following cycle 23 are likely to have low activity.

## 1. Introduction

22 The time-variability of solar activity indices, such as sunspot number and 10.7 cm radio  
23 flux, cycles with a period of about 11 years. The Sun begins a cycle at a minimum in  
24 the measured levels of activity indices, and ends at the next minimum. The familiar  
25 butterfly diagram shows both the regular 11-year cycle and the equator-ward drift of  
26 active regions. A primary understanding of the solar cycle has been established based  
27 on the theoretical model of a mean-field dynamo (Charbonneau 2005). However solar  
28 observations demonstrate more complexity than that can currently be modeled. The  
29 polar field during the minimum of cycle 23 was roughly 40% weaker than the previous  
30 three minima (e.g., Sheeley 2008; Kirk et al. 2009; Wang et al. 2009), and the extended  
31 and deep minimum of cycle 23 has attracted great attention in solar terrestrial scientific  
32 community. The continued lower activity level of the current maximum phase of solar  
33 cycle 24 provides more questions on the mechanism and impact of the peculiar status  
34 of the Sun on the Earth's space environment. To explore the many faces of solar cycle  
35 becomes a key task for solar astronomers.

36 The 11-year solar cycle was primarily defined by the number changes of sunspots  
37 (Schwabe 1844) and their latitudinal distribution (Maunder 1922). However, the sunspots  
38 are the manifestation of strong magnetic field which is structured and clustered into  
39 sunspots. With increasing spatial and temporal resolutions in solar observations, out-  
40 side of solar active regions, there appear many small-scale magnetic structures, such as  
41 ephemeral regions (Harvey and martin 1973), network (Sheeley 1966, 1967) and intra-  
42 network magnetic fields (Livingston and Harvey 1975; Smithson 1975). The solar mag-

netic field has shown a dichotomy in intrinsic field strength (Wang et al. 1995; Schrijver and Zwaan 2000; Jin et al. 2012) and an extremely rich spectrum in magnetic flux (Zhou et al. 2013). It appears as discrete flux patches and/or elements, from tiny magnetic elements of only  $10^{16}$  Mx to large flux patches with more than  $10^{21}$  Mx (Wang et al. 1985, 1995; Zhou et al. 2013).

Pioneering studies of solar cycle changes of magnetic flux in ephemeral regions have been carried out by Harvey and Harvey (1974), Harvey (1989), Harvey and Zwaan (1993), and Hagenaar et al. (2003), while for the magnetic network by Labonte and Howard (1982), Hagenaar et al. (2003), and Meunier (2003). On one hand, a few studies found that more ephemeral regions appeared during active solar condition (Harvey and Harvey 1974; Harvey 1989; Harvey and Zwaan 1993), and the number and magnetic flux of network concentration also increased (Meunier 2003) in this period. However, on the other hand, there are also studies pointing out no cyclic variation of network magnetic flux (Labonte and Howard 1982). Using six data sequence of 1996-2001 from SOHO/MDI full disk observations, Hagenaar et al. (2003) found that the cycle variation in emergence frequency of small ephemeral regions was in anti-phase with sunspot cycle, while the flux spectrum and the total absolute flux are independent of sunspot cycle for network concentration with fluxes  $\leq 20 \times 10^{18}$  Mx, and in phase with sunspot cycle for network concentration with fluxes from  $20 \times 10^{18}$  Mx to  $33 \times 10^{18}$  Mx. Based on the full disk magnetograms from SOHO/MDI covering an entire solar cycle 23, Jin et al. (2011) and Jin and Wang (2012) made a comprehensive analysis on the solar cycle behavior of the Sun's magnetic network elements. They found that with increasing flux per network element, the temporal variations of number and total flux showed a three-fold scenario: no correlation, anti-

66 correlation and correlation with sunspots. This is the first time that three categories of  
67 network magnetic structures are found, and the sources of these magnetic structures are  
68 explored and discussed.

69 In this paper, our goal is to understand how the flux spectrum changes during a solar  
70 cycle, in particular, the behavior of magnetic features with different magnetic flux during  
71 cycle 23. In this approach we extend our previous analysis to active region magnetic  
72 structures. We try to understand the cycle changes of all the magnetic structures in  
73 the flux spectrum, ranging from  $10^{18}$  Mx (the detectable smallest flux with SOHO/MDI  
74 measurements) to the largest coherent magnetic structures with flux of  $10^{22}$  Mx in active  
75 regions, and explore the difference of the extended minimum of cycle 23 from the minima  
76 of other solar cycles. The study is based on the analysis of both the sunspot number and  
77 magnetic flux. The observations and data analysis are described in Section 2. In Section  
78 3, we study the cycle variation of magnetic flux spectrum for all the observed magnetic  
79 structures. We compare the characteristics of the solar minimum in cycle 23 with that  
80 of all cycles since the first directly observed solar cycle (beginning at the year 1755) in  
81 Section 4. The conclusion and discussion are summarized in Section 5.

## 2. Observations and data analysis

82 SOHO/MDI observations provide the full disk 5-min average magnetograms with a res-  
83 olution of 2 arcseconds. We extract one magnetogram per day from 1996 September to  
84 2011 January, giving a total of 4022 magnetograms. For each magnetogram, we smooth  
85 it to reduce the noise level, and we correct the magnetic flux density for observed mag-  
86 netogram by assuming that the observed line-of-sight magnetic field is a projection of  
87 intrinsic magnetic field normal to the solar surface (Hagenaar et al. 2003; Jin et al. 2011;

88 Jin and Wang 2012). In addition, when the distance of a given pixel from solar disk center  
89 is larger than 60 degrees, the magnetic field of this pixel is set to zero. An example of  
90 data analysis is shown in Figure 1.

91 By analyzing the distribution function of magnetic signal in these magnetograms, we  
92 determine the noise level of 6 G. For each smoothed and corrected full disk magnetogram,  
93 we compute the total magnetic flux by taking the noise level threshold into account.  
94 For the identification of magnetic structures, we apply the magnetic field of 9 G ( $1.5\sigma$ )  
95 as a threshold, and all the signals below 9 G are set to zero to create the mask for each  
96 magnetogram. In the mask, there are many isolated pixels and small clusters, and then we  
97 remove them by using an IDL function ‘erode’. We define the magnetic concentration with  
98 area more than 10 square pixels (equaling to an area of 40 square arcsec) as a magnetic  
99 structure, and the examples of identified magnetic structures are shown in Figure 1. The  
100 identifying method of magnetic structures has been described in detail by Hagenaar et al.  
101 (2003) and Jin et al. (2011).

### 3. Cycle variation of magnetic flux spectrum

102 In total, we identify 11.5 million magnetic structures, which include active features  
103 and network magnetic elements. For these identified magnetic structures, we sort them  
104 according to their magnetic flux, and then we obtain the annual probability distribution  
105 function (PDF) and then get the average PDF during the entire solar cycle. In order  
106 to highlight the annual changes of the PDFs of different magnetic structures during the  
107 solar cycle, we compute the differential PDF (DPDF), i.e., the difference between the  
108 annual PDF and the average PDF in the entire solar cycle. The variation of magnetic  
109 flux spectrum is illustrated in Figure 2 from 1996 to 2010.

110 From the solar minimum to the solar maximum, the distributions of network magnetic  
 111 structures with flux ranging from  $\sim 2.5 \times 10^{18}$  Mx to  $\sim 4.0 \times 10^{19}$  Mx gradually decrease,  
 112 and reach the minimum in the years of 2000, 2001, and 2002. In the following years of the  
 113 cycle, their distributions gradually increase, and reach the maximum in the years of the  
 114 sunspot minimum. The number of magnetic structures in the flux range  $(2.5 - 40.0) \times$   
 115  $10^{18}$  Mx occupies 82% of all magnetic structures, and the distribution of these magnetic  
 116 structures shows clearly anti-correlated variation with sunspot cycle. On the contrary, the  
 117 distribution of magnetic structures with flux ranging from  $\sim 4.0 \times 10^{19}$  Mx to  $\sim 1.0 \times 10^{21}$   
 118 Mx shows the in-phase variation with the sunspot cycle. For the magnetic structures  
 119 with flux larger than  $10^{21}$  Mx, the changing of magnetic flux spectrum are not easy to be  
 120 identified due to their relatively small number. Therefore, in Figure 2, we enhance the  
 121 value of their DPDF by an order of magnitude, which are shown by the red dotted lines in  
 122 the figure. These magnetic structures in this flux range include features in active regions  
 123 and their surroundings. Obviously, the distribution of the magnetic structures with flux  
 124 larger  $10^{21}$  Mx shows the in phase variation with sunspot cycle. The number of in-phase  
 125 magnetic structures is 17% of all the magnetic structure. About 1% magnetic features  
 126 with flux in the range of  $(1.7 - 2.5) \times 10^{18}$  Mx, which is close to the observable limit of  
 127 magnetic feature by MDI instrument, they appear to not change during the entire solar  
 128 cycle. Because their number is very few and we also can not exclude the effects from the  
 129 instrument noise, we do not further analyze and discuss them in detail in this study.

130 For these correlated and anti-correlated magnetic structures, their spatial size range  
 131 covers each other partly. The area is in the range of  $(0.2 - 2.7) \times 10^{18}$  cm<sup>2</sup> (equalling to  
 132 the range from 40 square arcsec to 513 square arcsec) for these anti-correlated magnetic

133 features, and  $(0.3 - 33.8) \times 10^{18} \text{ cm}^2$  (equalling to the range from 57 square arcsec to 6425  
134 square arcsec) for these correlated magnetic features. Further, we analyze their cycle  
135 behaviors in terms of absolute total magnetic flux, which are shown in Figure 3. As a  
136 comparison, the total magnetic flux of full disk magnetogram and sunspot number are  
137 also displayed in the figure, which are plotted by black and red solid lines, respectively.  
138 Because the magnetic feature in this study is identified by magnetic flux concentration  
139 with size more than 10 pixels and magnetic field larger than 1.5 times of the noise level,  
140 a lot of magnetic flux are not considered in this analysis. Furthermore, it is more difficult  
141 to identify magnetic features during the solar minimum when the magnetic field is very  
142 low. Therefore, the sum of the magnetic flux for correlated and anti-correlated magnetic  
143 features is less than the magnetic flux of full disk magnetogram, and the ratio between  
144 them ranges from 59% to 93% from the Sun's minimum to maximum phase. Both the total  
145 flux and magnetic flux of correlated magnetic structures show an in-phase variation with  
146 sunspot cycle, and characterize a long-term transition between solar cycle 23 and 24. For  
147 the anti-correlated magnetic structures, their total magnetic flux reaches the minimum  
148 during sunspot number maximum, and vice versa. From 2007 October to 2009 December,  
149 the magnetic flux of anti-correlated magnetic structures is larger than that of correlated  
150 magnetic structures, and contributes 32.6%-37.8% magnetic flux to solar photosphere  
151 in this period, which is about 1.3 times of that contributed by the correlated magnetic  
152 structures. By the contributions of anti-correlated magnetic features, the magnetic flux  
153 in the cycle minimum is not too low, although there is a long spotless interval (over 500  
154 days) in this period.



155 In fact, from the solar minimum to maximum, the area of quiet region gradually de-  
156 creases with the emergence of more and more active regions, which will also result in the  
157 decrease of the number and magnetic flux for network magnetic structures. Therefore, by  
158 excluding the area of the active regions and then normalizing the quiet-Sun area, we check  
159 the result of the anti-correlated magnetic structures, which is shown in Figure 4 by the red  
160 symbol. As a comparison, the variation of anti-correlated magnetic structures without the  
161 normalization of the quiet-Sun area is also shown in the figure by the black symbol. We  
162 find that although there is some difference between the two-group data, the number and  
163 total magnetic flux of anti-correlated magnetic structures still show the anti-correlated  
164 variation with sunspots.

#### 4. The properties of extended minimum of solar cycle 23

165 For a better understanding the solar minimum of cycle 23, we extend the MDI data  
166 base by adding the Kitt Peak full disk magnetograms from 1996 August back to 1994  
167 January. The data merging is carried out by fitting the magnetic field from Kitt Peak  
168 magnetograms to that of MDI magnetograms for the common observations. The variation  
169 of total magnetic flux from 1994 January to 2011 January is shown in Figure 5, where the  
170 total magnetic flux obtained from Kitt Peak full disk magnetograms is displayed by green  
171 symbol. Here, we define the activity level with monthly average sunspot number less than  
172 20 as the low activity status of the Sun, which is displayed by the horizontal dotted line  
173 in Figure 5. We find that the duration of low activity status of cycle 22-23 is 27 months,  
174 i.e., from 1995 March to 1997 May. In this period, the magnetic flux falls in the range of  
175  $(1.1 - 1.5) \times 10^{23}$  Mx with an average magnetic flux of  $1.23 \times 10^{23}$  Mx. Comparing the  
176 duration of low activity status in solar cycle 22-23, the duration of low activity status in

177 solar cycle 23-24 is from 2006 January to 2010 September, which is 57 months long and  
178 30 months longer than that of cycle 22-23. In this period, the magnetic flux falls in the  
179 range of  $(1.0 - 1.7) \times 10^{23}$  Mx with an average magnetic flux of  $1.20 \times 10^{23}$  Mx, almost  
180 the same as that of cycle 22-23. It seems that the extended minimum of solar cycle 23 is  
181 characterized by the long-term low activity status but the magnitude of magnetic flux in  
182 the minimum period is not lower than the previous cycle.

183 In order to further understand the character of solar extended minima, we analyze the  
184 properties of solar minima in all solar cycles by studying the sunspot number changes. We  
185 adopt the monthly average sunspot number since 1755 (the first directly measured solar  
186 cycle), and apply a boxcar smoothing function to the sunspot number. Here, we define  
187 the minimum activity level of each solar cycle by the minimum sunspot number of the  
188 given cycle, i.e., the minimum value of monthly average sunspot number. We compute the  
189 duration of low activity status and minimum activity level for each solar cycle, which is  
190 shown in Figure 6. The black solid lines display the smoothing functions of the duration  
191 of low activity status and minimum activity level, which manifests the corresponding  
192 changing trend. As a comparison, the spotless days since solar cycle 9 are shown by red  
193 diamond symbol in Figure 6, whose magnitude is displayed by the right y-axis.

194 From Figure 6, it is clear that the minimum activity level in cycle 23 is obvious lower  
195 than that in cycle 22, and the duration of low activity status between solar cycles 23 and  
196 24 reaches the maximum in 100 years. In addition, we can find that the sunspot number  
197 seems to exhibit a century period approximately, i.e, Gleissberg solar cycle (Gleissberg  
198 1971), both in the duration of low activity status and the minimum activity level. From  
199 the distribution of minimum activity level, it can be found that the activity level in the

200 current century cycle is obvious stronger than the previous century cycle, but the current  
201 solar activity levels are lying in the weakening phase of current century cycle, which seems  
202 to indirectly confirm the results of grand maximum century cycle described by Usoskin  
203 et al. (2003), Solanki et al.(2004), Lockwood et al. (2009), and Lockwood (2013).

204 From the comparison among solar cycles in Figure 6, it can be found that the extended  
205 minimum of solar cycle 23 is similar with that of solar cycles 11 (the year around 1878)  
206 and 14 (the year around 1913). Moreover, from the distribution of the Gleissberg period,  
207 the solar cycles 11 and 23 appear to lie in the same phase, which seems to suggest the  
208 more similarity between solar cycles 11 and 23 than that for solar cycles 14 and 23 (lying  
209 in opposite phases in century cycle). Furthermore, the correlation coefficient of monthly  
210 sunspot number between solar cycles 11 and 23 reaches 0.98 with a very high confidence  
211 level, which is obviously larger than the correlation coefficient of 0.80 between solar cycles  
212 14 and 23. The correlation coefficient is the linear Pearson correlation coefficient computed  
213 by the covariance of the monthly sunspot number between two solar cycles.

214 We shrink or expand all solar cycles to the same time scale, and artificially divide  
215 each solar cycle into 130 bins. For the corresponding bins in solar cycles, we average the  
216 sunspot number to obtain an average solar cycle. The time scale of the average solar cycle  
217 is 10.9 years. We compare the average solar cycle with the three solar cycles with similar  
218 properties of solar minimum, i.e., solar cycles 11, 14 and 23, which is shown in Figure 7.  
219 For better visualization of solar cycle 23 and for forecasting future solar cycles, the solar  
220 cycle 11, 14 and average solar cycle have been overlaid relative to cycle 23. The solar  
221 cycle 14 shows the similar distribution to solar cycle 23 only during solar minima, but

222 solar cycles 11 and 23 reveal the similar sunspot distribution almost in the entire solar  
223 cycle as well as in the ascending and maximum phase of next solar cycle.

## 5. Conclusion and Discussion

224 Based on the unique database of full disk magnetograms obtained by SOHO/MDI from  
225 1996 September to 2011 January, we totally identify 11.5 million magnetic structures  
226 which include the observable smallest magnetic structures of SOHO/MDI to the magnetic  
227 structures of active regions, and study the variation of solar magnetic flux spectrum in  
228 solar cycle 23. By analyzing the sunspot numbers since solar cycle 1 and the magnetic  
229 flux changes in solar cycle 23, the properties of the extended minimum of cycle 23 are  
230 studied.

231 From the observable smallest magnetic structures to the magnetic structures of active  
232 regions, magnetic structures with different magnetic flux display different cycle behaviors:  
233 the magnetic structures with flux larger than  $4.0 \times 10^{19}$  Mx follow exactly the sunspot  
234 cycle, and show in phase variation with sunspots; while magnetic structures with a flux  
235 range of  $(2.5 - 40.0) \times 10^{18}$  Mx, which occupy 82% of total solar feature number, show  
236 an anti-correlation with sunspots. These results confirm our early studies (Jin et al.  
237 2011; Jin and Wang 2012) and agree mostly with the conclusion from Hagenaar et al  
238 (2003) by considering the underestimation of magnetic field in earlier MDI magnetogram  
239 calibration (Berger and Lites 2003; Wang et al. 2003) and 2008 December recalibration  
240 (see the detailed comparison in Jin et al. 2011).

241 During the low activity status of solar cycle 23-24, the average magnetic flux is  $1.20 \times 10^{23}$   
242 Mx with flux changes in the range  $(1.0 - 1.7) \times 10^{23}$  Mx. As a comparison, in the low  
243 activity status of cycle 22-23, the average magnetic flux is  $1.23 \times 10^{23}$  Mx with flux changes

244 in the range  $(1.1 - 1.5) \times 10^{23}$  Mx. There is a little difference of magnetic flux of cycle  
245 minima between the cycles 22-23 and 23-24. However, a few studies point out the 40%  
246 weaker of the polar field in the minimum of cycle 23-24 than that in the minimum of  
247 cycle 22-23 (e.g., Sheeley 2008; Kirk et al. 2009; Wang et al. 2009). According to the  
248 global dynamo model, the polar field comes from the poleward diffusion of magnetic flux  
249 of followed polarity active region. This seems to mean weaker magnetic flux of active  
250 region in cycle minimum 23-24 than that of cycle minimum 22-23. However, according to  
251 our analysis, there is little difference of the total magnetic flux during the two minima.  
252 A reasonable argument can only be that the magnetic structures of specific flux spectra,  
253 included in the flux transport and being responsible for creating the polar field in the  
254 minima of solar cycles 23-24, must have been less than that in the minima of cycles 22-23  
255 in their carrying magnetic flux. On the other hand, there must be a mechanism in a  
256 sense which generates magnetic flux in solar photosphere (i.e., the local dynamo), but  
257 the mechanism modulates or be modulated by the global dynamo (Jin et al. 2011; Jin &  
258 Wang 2012). Although there is a little difference of magnetic flux between the two cycle  
259 minima, the duration of low activity status in cycle 23-24 is more than 2 times longer  
260 than that in cycle 22-23. These results suggest that the extended minimum of solar cycle  
261 23 is characterized by the long-term low activity status but not the average magnetic  
262 flux during the low activity status. We further compute the duration of low activity  
263 status and the minimum activity level in term of the minimum sunspot number since the  
264 first solar cycle, and find that the sunspot number appears to exhibit a century period  
265 approximately, i.e., the Gleissberg period, both in the duration of low activity status and  
266 minimum activity level. The extended minimum of cycle 23 is similar to that of solar

267 cycle 11 considering both the properties of solar minimum and the phase of Gleissberg  
268 period. This similarity suggests that the solar cycles following solar cycle 23 could also  
269 be quite weak as that followed cycle 11.

### 270 **Acknowledgments.**

271 This work is supported by the National Basic Research Program of China  
272 (2011CB811403) and the National Natural Science Foundations of China (11003024,  
273 11373004, 11322329, 11221063, KJCX2-EW-T07, and 11025315).

### References

- 274 Berger, T. E., and Lites, B. W (2003), Weak-Field Magnetogram Calibration using Ad-  
275 vanced Stokes Polarimeter Flux Density Maps - II. SOHO/MDI Full-Disk Mode Cali-  
276 bration, *Sol. Phys.*, *213*(2), 213-229
- 277 Charbonneau, P. (2005), Dynamo Models of the Solar Cycle, *Living Rev. Sol. Phys.*, *2*(2)
- 278 Gleissberg, W. (1971), The Probable Behaviour of Sunspot Cycle 21, *Sol. Phys.*, *21*(1),  
279 240-245
- 280 Hagenaar, H. J., Schrijver, C. J., and Title, A. M. (2003), The Properties of Small Mag-  
281 netic Regions on the Solar Surface and the Implications for the Solar Dynamo(s), *ApJ*,  
282 *584*(2), 1107-1119
- 283 Harvey, K., and Harvey, J. (1974), A Statistical Study of Ephemeral Active Regions in  
284 1970 and 1973, *Bulletin of the American Astronomical Society*, *6*, 288-288
- 285 Harvey, K. (1989), The Solar Cycle Behavior of Small Active Regions, *Bulletin of the*  
286 *American Astronomical Society*, *21*, 839-839
- 287 Harvey, K. and Martin S. F. (1973), Ephemeral Active Regions, *Sol. Phys.*, *32*(2), 389-402

- 288 Harvey, K. and Zwaan, C. (1993), Properties and emergence of bipolar active regions, *Sol.*  
289 *Phys.*, *148*, 85-118
- 290 Jin, C. L., Wang, J. X., Song, Q., and Zhao, H. (2011), The Sun's Small-scale Magnetic  
291 Elements in Solar Cycle 23, *ApJ*, *731*(1), 37-45
- 292 Jin, C. L., and Wang, J. X. (2012), The Latitude Distribution of Small-scale Magnetic  
293 Elements in Solar Cycle 23, *ApJ*, *745*(1), 39-45
- 294 Jin, C. L., Wang, J. X., and Xie, Z. X (2012). Solar Intranetwork Magnetic Elements:  
295 Intrinsically Weak or Strong?, *Sol. Phys.*, *280*(1), 51-67
- 296 Kirk, M. S., Pesnell, W. D., Young, C. A., Hess Webber, S. A. (2009), Automated detec-  
297 tion of EUV Polar Coronal Holes during Solar Cycle 23, *Sol. Phys.*, *257*(1), 99-112
- 298 Labonte, B. J., and Howard, R. (1982), The magnetic flux in the quiet sun network, *Sol.*  
299 *Phys.*, *80*, 15-19
- 300 Livingston, W. C., and Harvey, J (1975), A New Component of Solar Magnetism - The  
301 Inner Network Fields, *Bulletin of the American Astronomical Society*, *7*, 346-346
- 302 Lockwood, M., Rouillard, A. P., and Finch, I. D. (2009), The Rise and Fall of Open Solar  
303 Flux During the Current Grand Solar Maximum, *ApJ*, *700*, 937-944
- 304 Lockwood, M. (2013), Reconstruction and Prediction of Variations in the Open Solar  
305 Magnetic Flux and Interplanetary Conditions, *LRSP*, *10*, DOI:10.12942
- 306 Maunder, E. W. (1922), The sun and sun-spots, 1820-1920, *MNRAS*, *82*, 534-543
- 307 Meunier, N. (2003), Statistical properties of magnetic structures: Their dependence on  
308 scale and solar activity, *A&A*, *405*, 1107-1120
- 309 Schrijver, C. J. and Zwaan C.(2000), Solar and stellar magnetic activity, *Cambridge Uni-*  
310 *versity Press*

- 311 Schwabe, M.(1843), Die Sonne. Sonnenbeobachtungen im Jahre 1843 Von Herrn Hofrath  
312 Schwabe in Dessau, *Astron. Nachr.*, *21*, 233-234
- 313 Sheeley, N. R., Jr. (1966), Measurements of Solar Magnetic Fields, *ApJ*, *144*, 723-735
- 314 Sheeley, N. R., Jr. (1967), Observations of Small-Scale Solar Magnetic Fields, *Sol. Phys.*,  
315 *1*(2), 171-179
- 316 Sheeley, N. R., Jr. (2008), A Century of Polar Faculae Variations, *ApJ*, *680*(2), 1553-1559
- 317 Smithson, R. C. (1975), Observations of Weak Solar Magnetic Fields with the Lockheed  
318 Diode Array Magnetograph, *Bulletin of the American Astronomical Society*, *7*, 346-346
- 319 Solanki, S. K., Usoskin, I. G., Kromer, B., Schüssler, M., and Beer, J. (2004), Unusual  
320 activity of the Sun during recent decades compared to the previous 11,000 years, *NA-*  
321 *TURE*, *7012*, 1084-1087
- 322 Usoskin, Ilya G., Solanki, Sami K, Schüssler, Manfred, Mursula, Kalevi, and Alanko, Katja  
323 (2003), Millennium-Scale Sunspot Number Reconstruction: Evidence for an Unusually  
324 Active Sun since the 1940s, *PhRvL*, *91*, id.211101
- 325 Wang, J. X., Wang, H. M., Tang, F., Lee, J. W., and Zirin, H. (1995), Flux distribution  
326 of solar intranetwork magnetic fields, *Sol. Phys.*, *160*(2), 277-288
- 327 Wang, J., Zirin, H., and Shi, Z. Tang, F. (1985), The smallest observed elements of  
328 magnetic flux, *Sol. Phys.*, *98*(2), 241-253
- 329 Wang, J. X., Zhou, G. P., Wang, Y. M., and Song, L. M. (2003), Circular Polarization in  
330 a Solar Filament, *Sol. Phys.*, *216*(1), 143-157
- 331 Wang, Y. M., Robbrecht, E., and Sheeley, N. R. Jr (2009), On the Weakening of the Polar  
332 Magnetic Fields during Solar Cycle 23, *ApJ*, *707*(2), 1372-1386



<sup>333</sup> Zhou, G. P., Wang, J. X., and Jin, C. L. (2013), Solar Intranetwork Magnetic Elements:  
<sup>334</sup> Flux Distributions, *Sol. Phys.*, *283*(2), 273-282

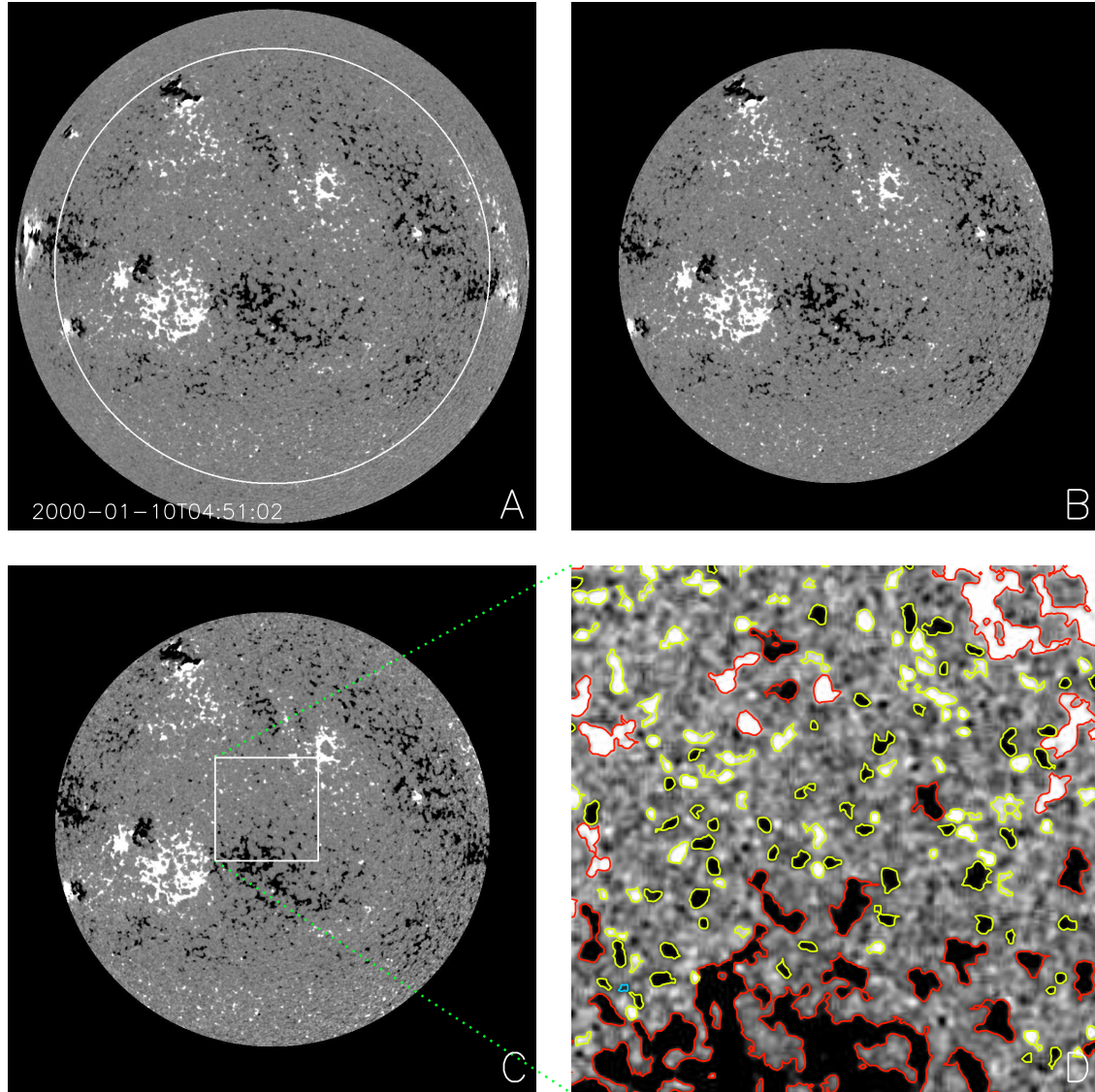


**Figure 1.** Panel A: The 5-min average full disk magnetogram from MDI. The white solid line means the boundary of 60 degrees. Panel B: The same magnetogram with panel A, but for these pixels far away from solar disk center larger than 60 degrees being masked out. Panel C: The same magnetogram with panel B, but the observed magnetic field being corrected by projection assumption. Panel D: The magnetogram central square highlighted in panel C, shown in expanded view. The three categories magnetic structures are highlighted by different colors. The in-phase magnetic structures are contoured by red lines, anti-correlated magnetic structures by yellow lines, and no-correlated magnetic structures by blue lines.

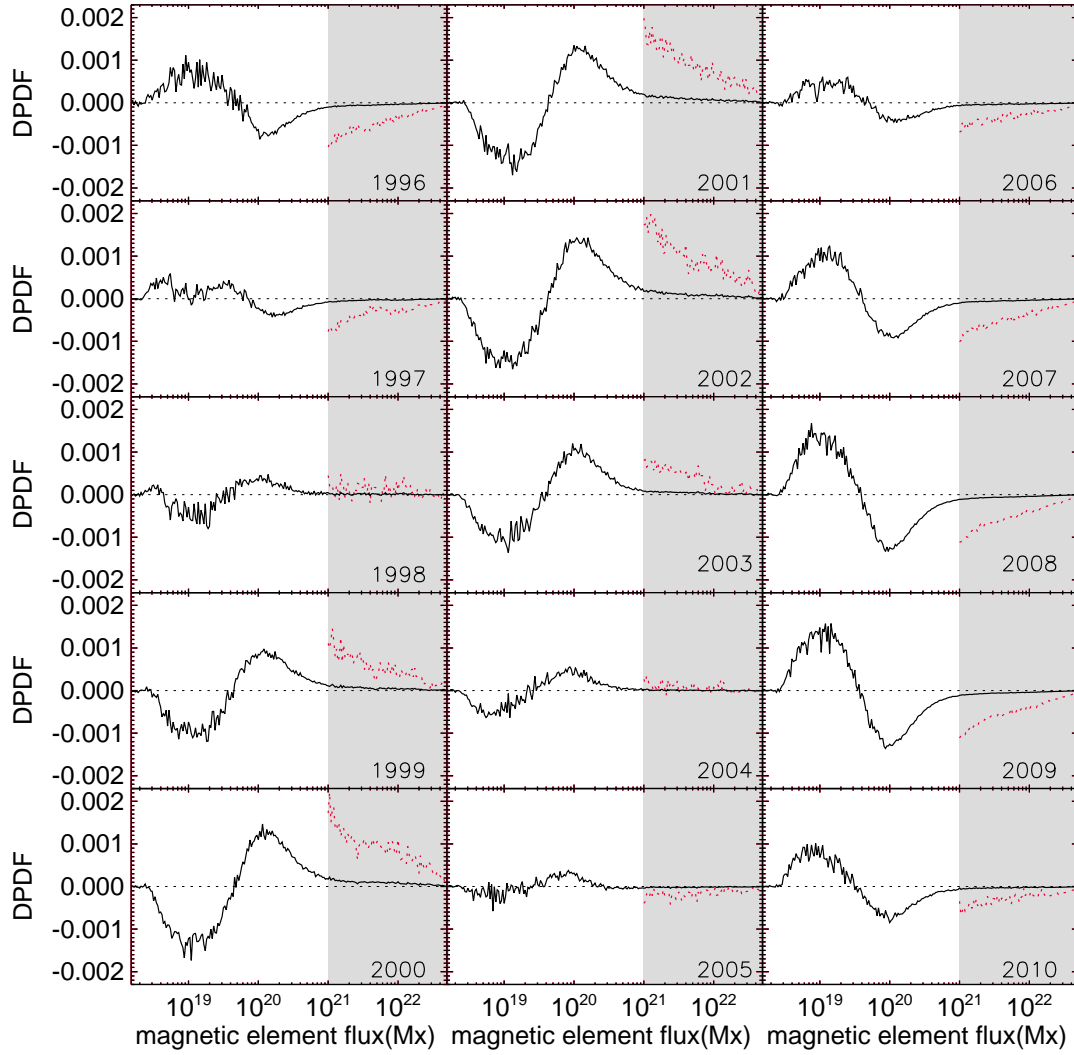


**Figure 2.** The cycle variation of magnetic flux spectrum from the observed smallest magnetic structures to magnetic structures of active regions. The DPDF value of the magnetic structures with flux larger than  $10^{21}$  Mx in the gray background is enlarged by a factor of 10, which is plotted by the red dotted line.

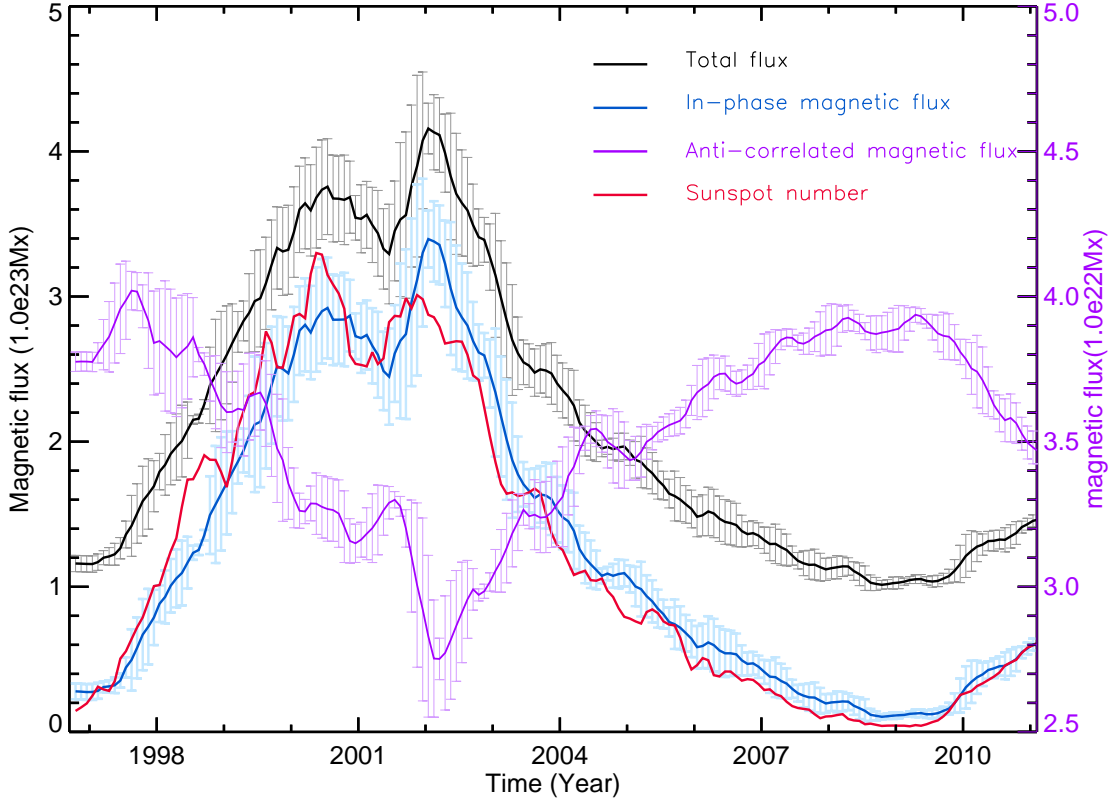


**Figure 3.** The cycle variations of smoothed total magnetic flux for in-phase (the magnitude is shown by left y-axis) and anti-correlated (the magnitude is shown by right y-axis) magnetic structures. As a comparison, the variations of smoothed full disk magnetic flux (the magnitude is shown by left y-axis) and sunspot number are also plotted by the black and red solid lines. The vertical lines show the corresponding error bar.

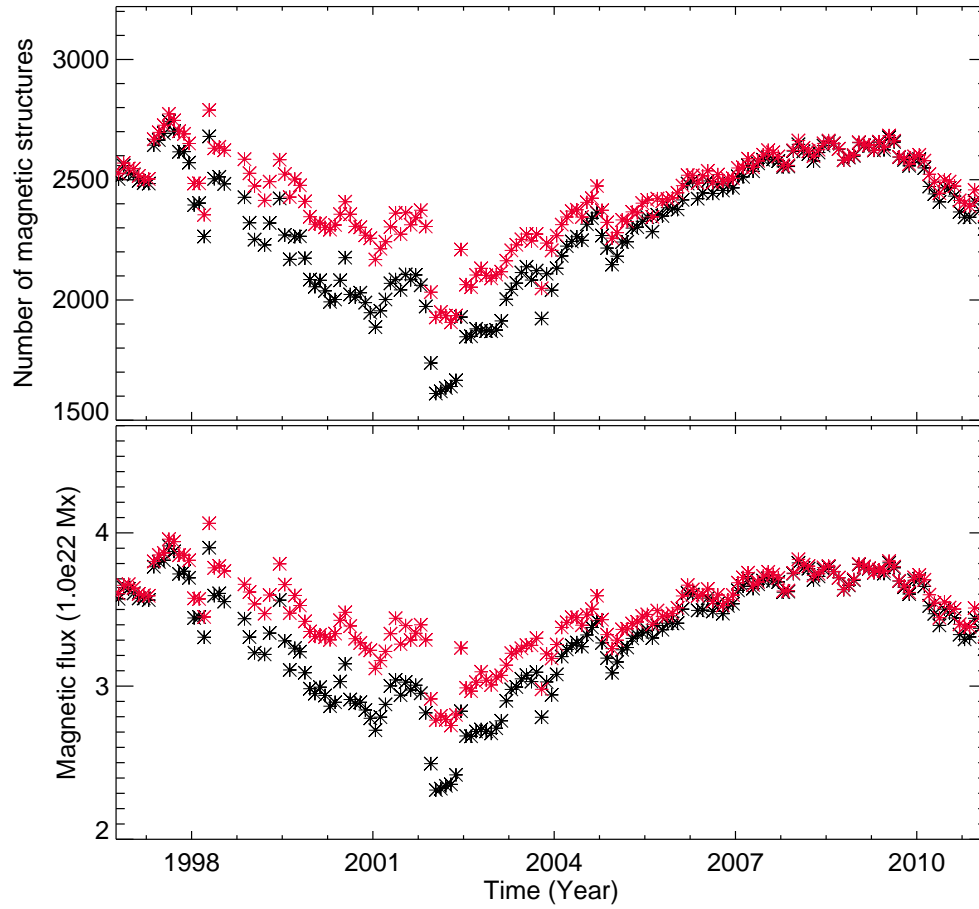


**Figure 4.** The cycle variation of anti-correlated magnetic structures. The top panel displays their number variation, and the bottom panel indicates their magnetic flux variation. The data points displayed by red symbol are corrected by normalizing the quiet-Sun area, but the data points showed by black symbol are not corrected.

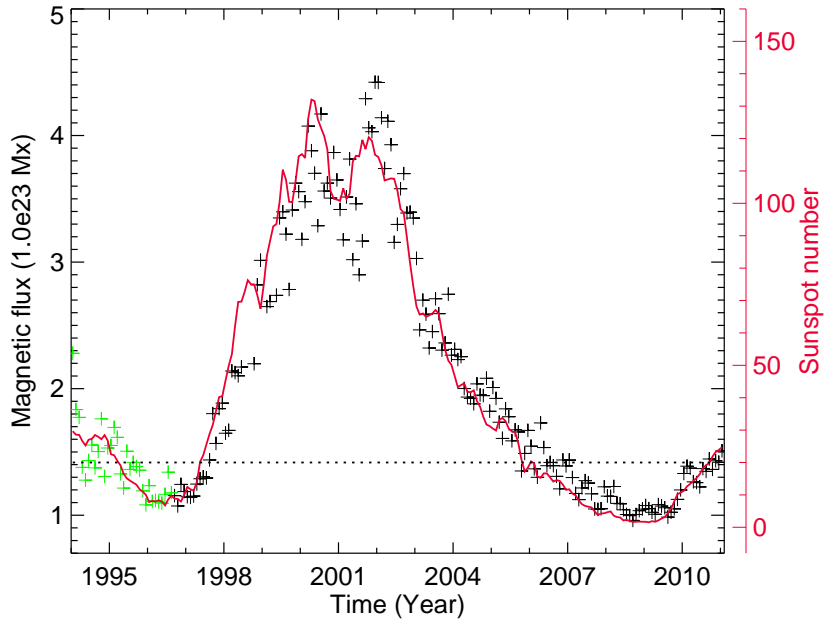


**Figure 5.** The cycle variations of full disk total magnetic flux. The green ‘+’ symbol data points mean the magnetic flux calculated by the Kitt Peak full disk magnetograms, while the black ‘+’ symbol data points show the magnetic flux obtained from MDI full disk magnetograms. The red solid line means the sunspot number, whose value is shown by the right y-axis. The sunspot number less than 20, shown by the horizontal dotted lines, represent the Sun’s low activity status.

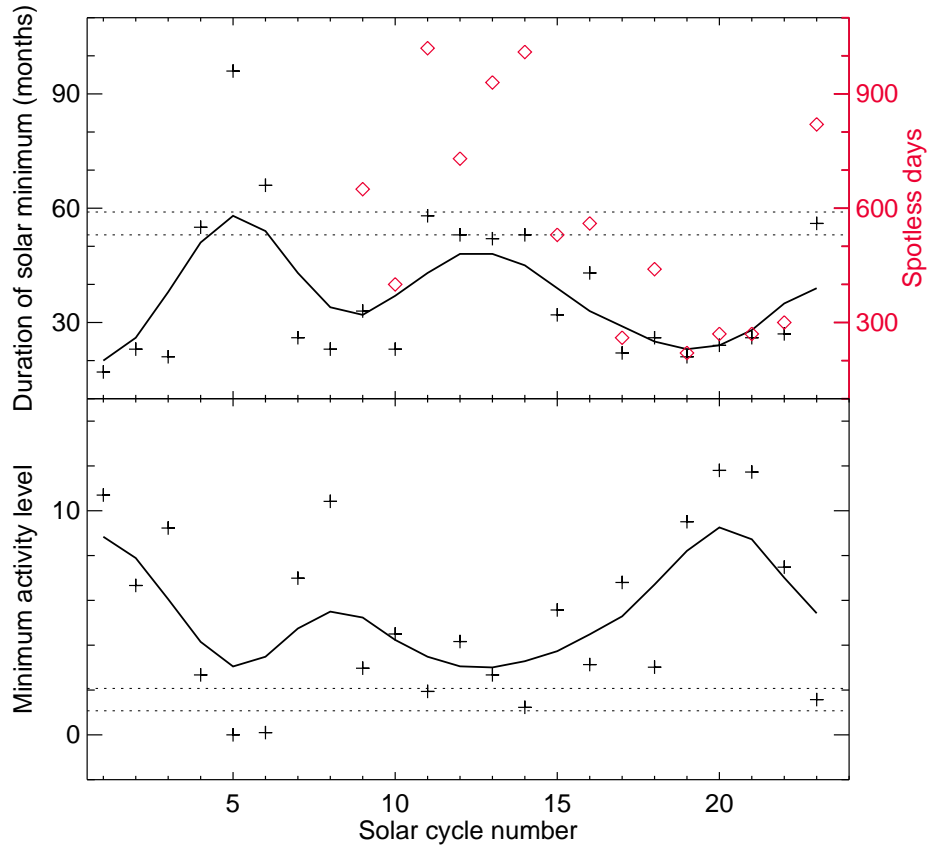


**Figure 6.** The properties of solar minimum since the solar cycle 1 (beginning at the year of 1755). The x-axis means the serial number of solar cycle. The data points within the horizontal dotted lines mean that the corresponding solar cycles have the similar minimum activity level and duration of solar minimum activity status with solar cycle 23. The black solid lines mean the changing trends of minimum activity level and duration of minimum activity status. The red diamond symbols mean the spotless days in the corresponding solar cycle.

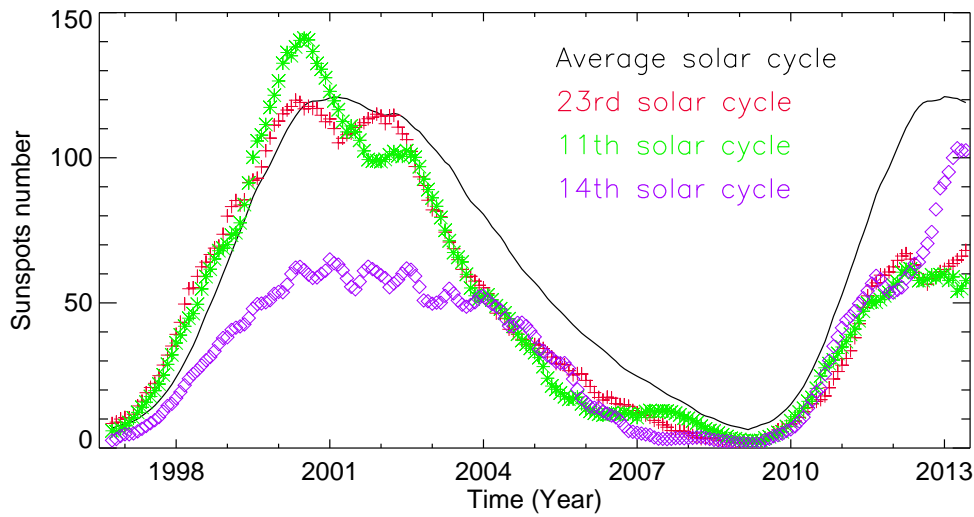


**Figure 7.** The comparison among the average solar cycle, solar cycles 11, 14, and 23 by analyzing sunspot number. The time scales of average solar cycle, solar cycles 11 and 14 have been expanded or shrunk according to the time span of solar cycle 23.